

RSC Advances



This is an *Accepted Manuscript*, which has been through the Royal Society of Chemistry peer review process and has been accepted for publication.

Accepted Manuscripts are published online shortly after acceptance, before technical editing, formatting and proof reading. Using this free service, authors can make their results available to the community, in citable form, before we publish the edited article. This *Accepted Manuscript* will be replaced by the edited, formatted and paginated article as soon as this is available.

You can find more information about *Accepted Manuscripts* in the [Information for Authors](#).

Please note that technical editing may introduce minor changes to the text and/or graphics, which may alter content. The journal's standard [Terms & Conditions](#) and the [Ethical guidelines](#) still apply. In no event shall the Royal Society of Chemistry be held responsible for any errors or omissions in this *Accepted Manuscript* or any consequences arising from the use of any information it contains.

A multifunctional multi-walled carbon nanotubes/ceramic membrane composite filter for air purification

Yang Zhao,^a Zhaoxiang Zhong,^{*, a} Ze-Xian Low,^b Zhong Yao^a

^aState Key Laboratory of Materials-Oriented Chemical Engineering, National Engineering Research Center for Special Separation Membrane, NanjingTech University, Nanjing 210009, China

^bCentre for Advanced Separations Engineering and Membranes@Bath, Department of Chemical Engineering, University of Bath, Claverton Down, Bath BA2 7AY, United Kingdom

Abstract

Carbon nanotubes (CNTs) are very small diameter fibers that have the potential to be integrated into filters to further increase particle capture efficiency. In this work, we used a chemical vapor deposition (CVD) method to create the carbon nanotubes/ceramic composite filter by growing multi-walled carbon nanotubes (MWCNTs) on a porous alumina ceramic membrane. Compared with the pristine alumina ceramic membrane, although the mean pore size and porosity of composite filter decreased 9.2% and 11.0% respectively, the resulting composite filter showed significant improvements in air filtration performance, owing to the dramatical increase of specific area by two order of magnitude and enhancement of wall slip flow effect over CNTs. The pressure drop across the composite filters decreased about 62.9% with respect to that of the pristine filters, while the filtration efficiency of the composite filters at the most penetrating particle size (MPPS) has been increased to 99.9999% (reached the standard of ULPA filters), leading to an obvious higher quality factor (Q_f). The presence of CNTs strongly inhibits the propagation of bacteria on the filters with an antibacterial rate of 97.86% and show high water repellency (water contact angle of 148.2°). These results make the composite filter very promising for multifunctional air filtration applications.

Introduction

Air pollution is one of the most serious global problems threatening the human health.¹ The polluted air containing submicron particles, nanoparticles and germs can cause various diseases including acute illnesses, chronic diseases, systemic poisoning or even death.²⁻⁴ Reduction or complete

removal of these harmful substances are needed and can be achieved using air filters.⁵ Two standards were established for evaluating the filtration performances of air filters — High-efficiency particulate air (HEPA) and ultra-low penetration air (ULPA). As defined, HEPA filters and ULPA filters have filtration efficiency (retention rate) of >99.97% and >99.9995%, respectively for air particles of size 0.3 μm or larger.⁶⁻⁸ Air filters remove the aerosol particles via five established mechanisms: Brownian diffusion, direct interception, inertia impact, gravity settling, and electrostatic deposition, of which they change with the filtration conditions.⁶ Pressure drop is one of several parameters that needs to be controlled in air filtration process.⁵⁻⁶ High pressure drop is undesired as it increases the overall energy consumption of the air filtration process (about 70% of total energy).⁶ There exists a trade-off between the retention rate and pressure drop in traditional single phase filter.⁶ In order to break the trade-off and to achieve higher retention rate with lower pressure drop, several nanomaterials have been investigated for application in air filtration including ZnO and carbon nanotubes (CNTs).⁹⁻¹¹ CNTs have been traditionally studied for various applications in fuel cell, water treatment, liquid and gaseous clean-up.^{5, 12-15}

Chemical vapor deposition (CVD) method is one of the most popular route for the preparation of CNTs and has been used to fabricate nanocomposite filters by growing CNTs on different substrates.¹⁶⁻¹⁸ Among the substrates, ceramic-based membranes have been widely studied due to their superior inherent properties including chemical, mechanical and thermal stability.¹⁹⁻²⁰ The excellent stability of the ceramic membranes can ensure the stable physic-chemical property of the composite filter, and can be essential for the preparation of composite membranes by CVD method.²¹ However, ceramic membranes consist of randomly interconnected pore structure in diverse directions could lead to high pressure drop when used as air filters.^{5, 22} Growing of CNTs on ceramic membranes on the other hand, could lead to desirable air filtration performance. Microorganisms like bacteria in the air causes public concerns about health.²³⁻²⁴ Nano-sized substances such as CNTs and Ag nanoparticles have the antibacterial property since they can cause damages of bacterial cell membrane or enter into the interior of the bacteria cell through cell membrane and affect the cell division process.^{25-27, 49} Traditional air filters are also susceptible to microorganism contamination, which not only impacts the lifespan of the filters but also reduces the quality of air purification caused by deposition of bacteria in the filter.²⁸ Therefore, much effort is still needed in search of a multifunctional filter with stable physic-chemical property, high particulate removal efficiency, low

pressure drop, and anti-bacterial property.

In the present study, we fabricated a multifunctional air filter by using CVD method to grow CNTs on the porous alumina membranes to break the trade-off between the retention rate and pressure drop, and exploit the anti-bacterial properties of CNTs. The filtration performance was studied under different experimental conditions. The antibacterial property and wettability of the composite membranes were also investigated to understand the effectiveness of incorporating CNTs in alumina membranes.

Experimental

Materials

Alumina ceramic membranes were produced in-house and used as is (thickness: 1 – 3 mm, Φ 30mm, mean pore size: 3.24 μm , Porosity: 53.19%). Xylene (C_8H_{10} , purity $\geq 99.0\%$) and acetone ($\text{C}_3\text{H}_6\text{O}$, purity $\geq 99.5\%$) were purchased from Shanghai Lingfeng Chemical Reagent Co., Ltd., China. High purity nitrogen (N_2 , purity $> 99.999\%$) was purchased from Nanjing Sanle Electronic Information Industry Group Co., Ltd., China and used as received. NaCl (purity $\geq 99.5\%$) and NaOH (purity $\geq 96\%$) were supplied by Sinopharm Chemical Reagent Co., Ltd., China. Ferrocene ($\text{FeC}_{10}\text{H}_{10}$) was used as the catalyst and was purchased from Aladdin Industrial Corporation Shanghai, China. Isopropyl alcohol ($(\text{CH}_3)_2\text{CHOH}$, purity $\geq 99.7\%$) was purchased from Shanghai Shenbo Chemical Co., Ltd., China. Tryptone LP0042 and yeast extract LP0021 were purchased from Oxoid, Ltd., Basingstoke, Hampshire, England, and agar ($(\text{C}_{12}\text{H}_{18}\text{O}_9)_n$) was purchased from Biosharp, Japan.

Fabrication of MWCNTs/ceramic membrane composite filter

Alumina ceramic membranes were first ultrasonicated in acetone for 20 min. The alumina ceramic membranes were then boiled in water for 30 min for further removal of the impurities including acetone on the surface of the membrane. The alumina ceramic membranes were subsequently dried in a vacuum drying oven for 24 h at 60 °C.

The process for the fabrication of carbon nanotubes/ceramic composite filter is shown in Fig. S1 (supporting information). First, 1.5 g ferrocene was dissolved in 50 ml xylene. The cleaned alumina ceramic membrane was placed in the center of a quartz tube (i.d. 40 mm), which was placed in a

horizontal tube furnace. N₂ was introduced into the tube at a flow rate of 15 ml/s for 5 min in order to flush out the air in the tube. The temperature controller was then set up from 25°C to 850°C within 30 min, and the reaction temperature was maintained at 850°C for 60 min. Once the inside temperature of the quartz tube reached 850°C, we changed the flow rate of N₂ to 10 ml/s, and injected the mixed solution of xylene and ferrocene into the tube at a rate of 0.3 ml/min for 60 min for the growth of multi-walled carbon nanotubes (MWCNTs) on the alumina ceramic membrane matrix. After the end of the reaction, the furnace was cooled to room temperature under the flow of N₂ at a rate of 15 ml/s. The MWCNTs/ceramic membrane composite filter was obtained.

Material Characterization

We used field emission scanning electron microscopy (FESEM, Hitachi S-4800, 15 kV) and transmission electron microscopy (TEM, JEM-2100, HR at 200 kV) to characterize the morphology of the pristine alumina ceramic membrane and carbon nanotubes/ceramic composite filter. For TEM sample preparation, the composite filter was milled into powder in a mortar, and then we sonicated this powder in isopropyl alcohol for 20 min, 100 W before transferring a drop of the suspension onto a carbon-coated copper grid. The Raman spectroscopy of MWCNTs removed from the filters with scratching was measured by Labram HR (Horiba, 5 mW, $\lambda = 514$ nm). The contact angle of water of the filters was studied using a video based contact angle measuring device (DropmeterTM, A100). The mean particle size and size distribution of SiO₂ particles were measured using Sysmex FPIA-3000. Gas permeability, pore size of the pristine filter and composite filter were measured by pore-size distribution analyzer (wetting agent: water, testing area: 0.2 cm², Specimen thickness: 1.5 mm, GaoQ, PSDA-20). The number concentration of aerosol SiO₂ particles was measured by DustTrakTM II aerosol monitor 8530. Gravimetric method was used for determining the porosity of all test materials, and the porosity was calculated as:

$$\text{Porosity(\%)} = (\text{wet weight} - \text{dry weight}) / (\text{wet weight} - \text{submerged weight}) \quad (1)$$

where wet weight is the weight of the completely water-wetted filter, dry weight is the weight of the dry filter, and the submerged weight refers to the weight of the filters by the buoyancy action of water. Both the pristine and the composite filters were completely wetted via vacuum filtration and further boiled in water for 3 h to ensure the filters were completely wetted before measuring the wet weight. Brunauer-Emmett-Teller (BET) surface areas were determined by using a surface area and

porosity analyzer (ASAP-2460). MWCNTs were scrapped from the surface of the composite filter for surface area analysis. The filter specific area was defined as:¹⁶

$$\text{Filter specific area} = \text{BET surface area} \times \text{Density} \quad (2)$$

Filtration performance test

The in-house filter testing rig for measuring the filtration efficiency and pressure drop of the filters is shown in Fig. 1. The filter was first placed in a filter holder. The carrier gas was supplied through an air bottle with adjustable flow rate of 0.5 – 4 cm/s by a gas flowmeter. The carrier gas was then passed through a box with SiO₂ powder to generate aerosol particles before entering the filter holder. The real-time number concentration of SiO₂ particles at the upstream and downstream of the pristine filter or the composite filter was detected by DustTrak™ II aerosol monitor 8530. At the same time, we recorded the value of pressure before and after filtration by Pressure transducers.

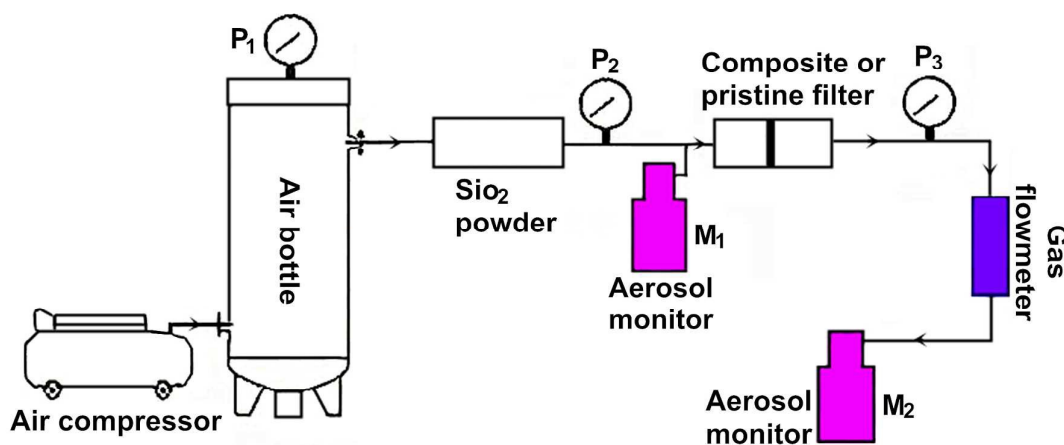


Fig. 1 Schematic diagram of air filtration performance test. P₁ is the pressure value of the air bottle, P₂ is the pressure value before the pristine or the composite filter, and P₃ is the pressure value after the pristine or the composite filter. M₁ and M₂ refer to the number concentration of SiO₂ particles before and after filtration, respectively.

The pressure drop of the pristine filter and the composite filter were determined by using the following equation:

$$\Delta P = P_3 - P_2 \quad (3)$$

where ΔP is the pressure drop. P₂ is the upstream pressure value, and P₃ is the downstream pressure

value. The retention rate (R) is defined as :

$$R (\%) = \left(1 - \frac{C_{\text{down}}}{C_{\text{up}}} \right) \times 100 \quad (4)$$

where C_{down} is the SiO_2 particles concentration measured downstream from the pristine filter or the composite filter, while C_{up} is the SiO_2 particles concentration measured upstream from the pristine filter or the composite filter. The quality factor (Q_f) was the criterion for comparing filtration performances with different filters, and it was defined as:

$$Q_f = \frac{-\ln P}{\Delta P} \quad (5)$$

$$P = \frac{M_1}{M_2} = 1 - R \quad (6)$$

Where M_1 and M_2 represent the number concentration of SiO_2 particles measured downstream and upstream from the pristine or the composite filter, respectively and P is the value of penetration, which is usually used for filters with high filtration efficiency.^{16, 29}

Antibacterial test

Fig. S2 (supporting information) is the schematic of antimicrobial activity test. The antibacterial tests of the pristine filter and the composite filter were performed by using colony counting method.^{9,50} First, 10 g of tryptone, 5 g of yeast extract and 10 g of NaCl was dissolved in 1L of sterilized deionized water. The pH value of this mixed solution was adjusted to 7.0 by using 1 mol/ml NaOH, and it was sterilized in an autoclave for the preparation of nutrient broth. The constituents of nutrient agar solid medium were the same as the nutrient broth, and 15 g/L of agar was added. The bacterial suspension was prepared by incubating 1 ml culture inoculated in 200 ml of nutrient broth for 37 °C, 24 h. The pristine filter (2 g) and the composite filter (2 g), both milled into powder in a mortar, were placed into a test tube with *E.coli* suspension (15 ml, optical density 0.1) respectively. The *E.coli* would make contact with the pristine filter and the composite filter respectively in their own test tube at 37 °C, 180 RPM for 40 min. After the shaking incubation, the bacterial suspension was diluted to 100 times with sterile nutrient broth, and 100 µl of the diluted bacterial suspension was spread onto a

nutrient agar plate. The plate was incubated for 24 h at 37 °C in a biochemical incubator. After incubation, the colonies formed on the plate were counted. Viable cells formed colonies on the nutrient agar plates, while the dead cells caused by the antibacterial effect of the test samples did not.⁹ The antimicrobial activity test was repeated for shaking incubation time at 80 min and 120 min respectively in order to study the change of antibacterial property with different shaking incubation time. The antibacterial test for both the pristine filter and the composite filter with different shaking incubation time (40 min, 80 min, 120 min) were repeated for three times, and the mean value of antibacterial rate for both the pristine filter and the composite filter were taken.

The antibacterial rate for the pristine filter and the composite filter with different shaking incubation time (40 min, 80 min, 120 min) were determined using the following formula:

$$\text{Antibacterial rate} = \left(1 - \frac{A}{B}\right) \times 100\% \quad (7)$$

where A is the composite filter number of the colonies formed on the plate, and B is the pristine filter number of the colonies formed on the plate.

Results and discussion

Surface appearance and microstructure of the filters

The typical surface morphologies of the pristine filter and the composite filter are shown in Fig. 2a-b. The in-house alumina ceramic filter was porous and uneven, and wide pore size distribution was observed on the surface of the pristine filter. In Fig. 2b, the CNTs were well grown on the surface and around the pores of the composite filter, and the CNTs were curved and intertwined with each other. Although CNTs were grown on the composite filter, there were still some visible pores on the composite filter. Fig. 2c also verified that the MWCNTs did not cover all the pores of the composite filter. The TEM image (Fig. 2d) confirmed the growth of CNTs on the composite filter was hollow MWCNT with a wall thickness about 4.5 nm and inner diameter about 8.3 nm.

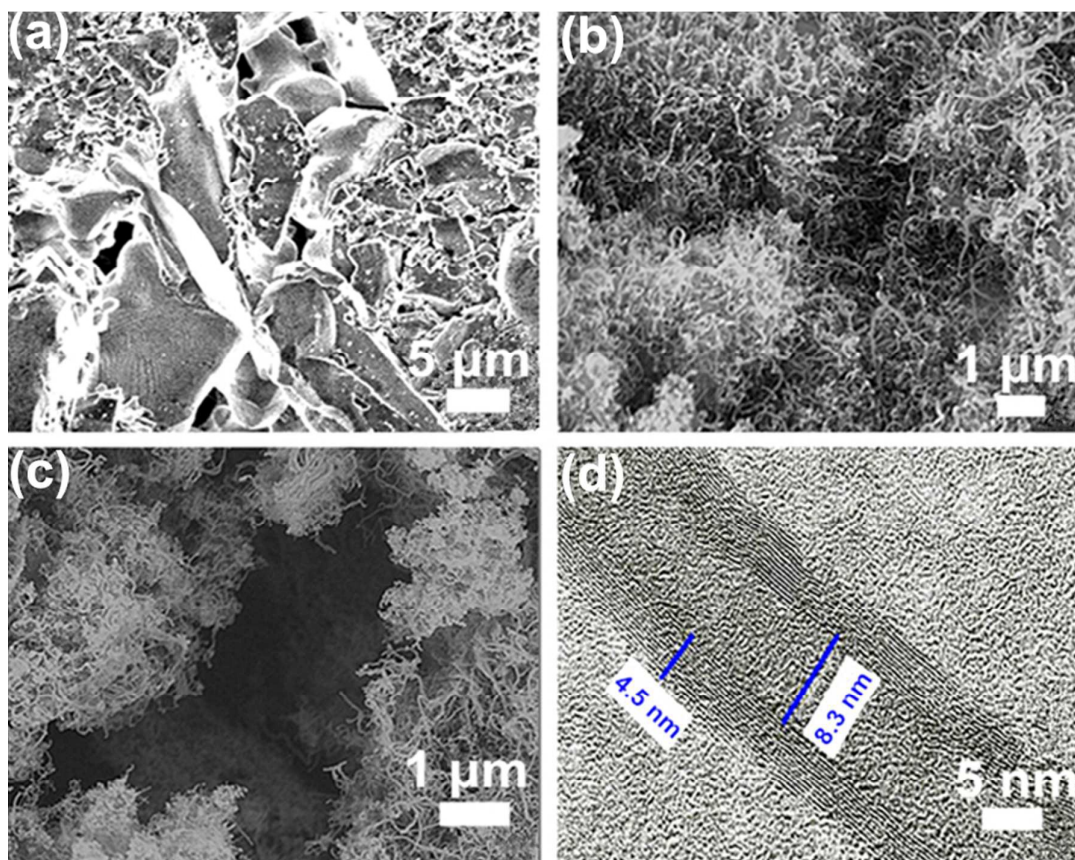


Fig. 2 (a) FESEM image of the pristine ceramic filter, (b) FESEM image of the CNTs/ceramic composite filter, (c) high magnification view of a pore of the composite filter, (d) TEM image of the MWCNT on the composite filter.

Raman spectroscopy is a powerful characterization tool for CNTs.³⁰ Fig. 3 shows the Raman spectrum of the CNTs removed from the composite filter. The three known peaks (D band, G band and G' band) of MWCNTs also verified that the CNTs grown on the composite filter were MWCNT.³¹⁻³² The intensity of the D band is proportional to the structural imperfections and impurities in MWCNTs, while the intensity of G band refers to the structural perfections and purities of MWCNTs.²⁵ The Raman intensity of D band (I_D) was weaker than the Raman intensity of G band (I_G), and $I_D / I_G = 0.54$, indicating that the MWCNTs grown on the composite filter have less deficiencies.

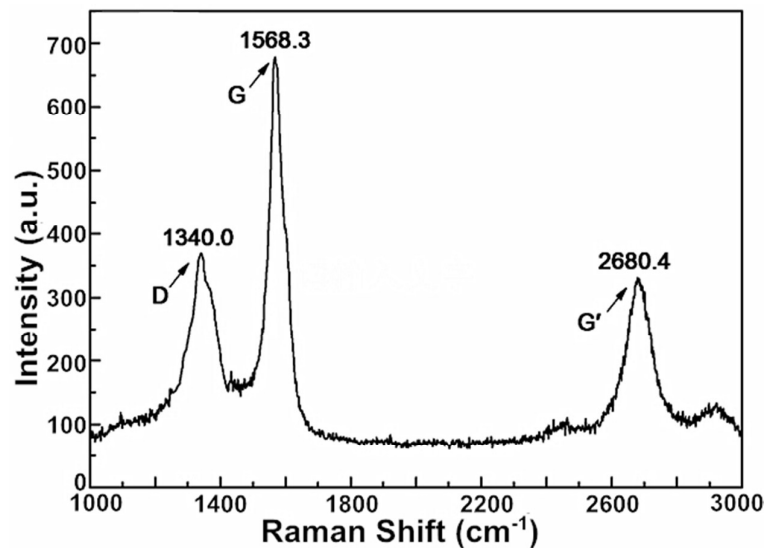


Fig. 3 Raman spectrum of the CNTs grown on the composite filter.

Characteristics of the pores and gas permeability of the filters

The mean pore size of the pristine filter was 3.24 μm . After CVD progress, MWCNTs were uniformly coated on the surface and around the pores of the composite filter (Fig. 2b), leading to lower mean pore size of the composite filter of 2.94 μm . The pore size distribution of the pristine filter and the composite filter are shown in Fig. 4a. The pore size of the pristine filter peaked at 3.3 μm , 63.7%, while the pore size of the composite filter peaked at 3 μm , 51.5%. The porosity of the pristine filter and the composite filter were 53.19% and 47.29% respectively. The mean pore size and porosity of the composite filter decreased compared with the pristine filter, owing to the growth of MWCNTs on the surface and around the pores of the composite filter (length about 2 μm , Fig. 2b-c), and the length of the MWCNTs was smaller than the mean pore size of the pristine filter (3.24 μm), leading to the pores on the composite filter were not completely covered (Fig. 2c).

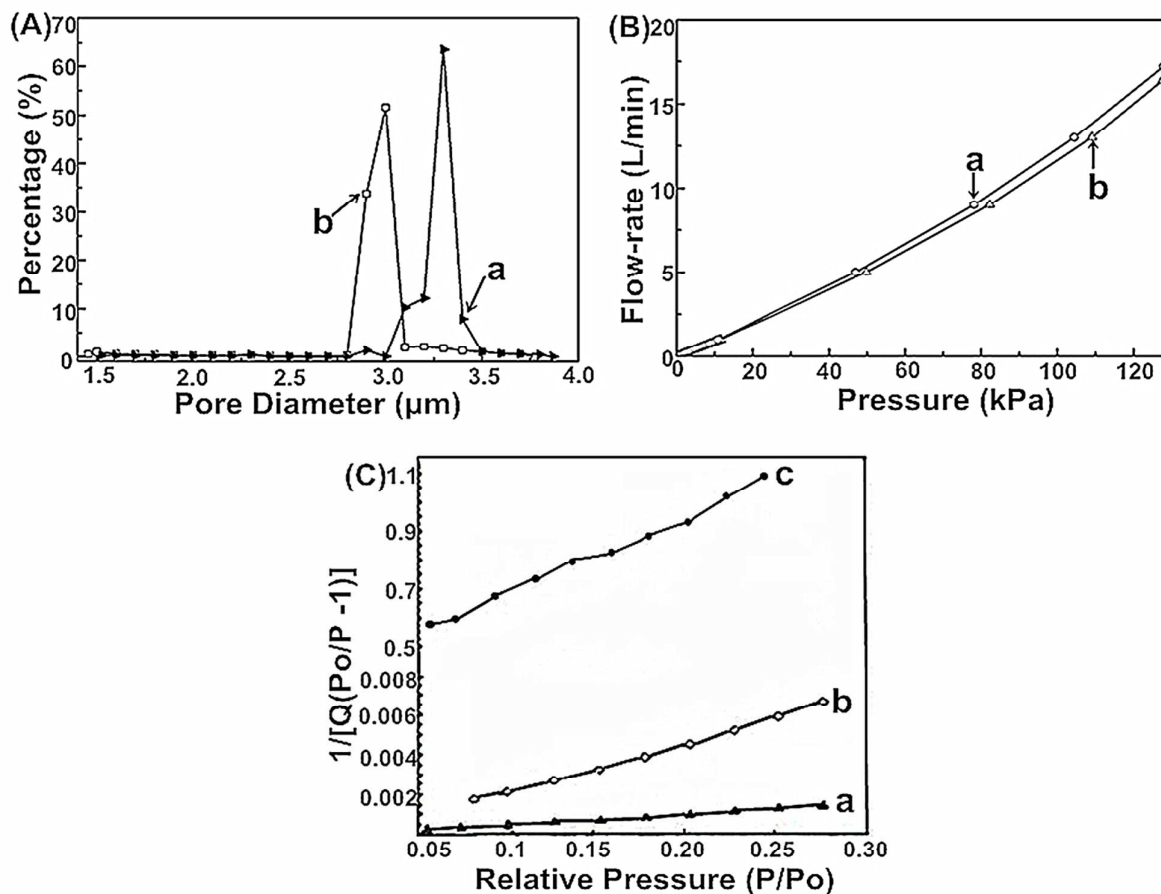


Fig. 4 (a) Pore size distribution of the pristine filter (a) and the composite filter (b), (b) The gas permeability of the pristine filter (a) and composite filter (b). (c) BET surface area plot. The pristine filter (a), the composite filter (b), and MWCNTs (c).

The gas permeability of the pristine filter and the composite filter are shown in Fig. 4b. Although the gas permeability of the composite filter was lower than the pristine filter with the rising pressure, there was no significant decrease compared with the pristine filter. The gas permeability of the pristine filter and the composite filter were $39080 \text{ m}^3/\text{m}^2 \text{ h bar}$ and $37440 \text{ m}^3/\text{m}^2 \text{ h bar}$ respectively. The slight reduction in gas permeability was due to growth of MWCNTs on the surfaces and the pores of the composite filter, leading to smaller pore size (Fig. 4a). However, the MWCNTs grown on the composite filter were hollow (Fig. 2d), and the gas could not only pass through the pores and space between the MWCNTs on the composite filter, but also through the hollow MWCNTs. Compared with the pristine filter, the slight decline of gas permeability was consistent with the small decrease of mean pore size and porosity of the composite filter.

Fig. 4c shows the BET surface area of the pristine filter, composite filter and pure MWCNTs.

The results showed that the BET surface area of the pristine filter, the composite filter and MWCNTs were 1.59 ± 0.04 , 176.75 ± 4.36 and 818.79 ± 20.05 m²/g respectively. The large BET surface area of MWCNTs made a great contribution to increase the BET surface area of the composite filter (from 1.59 ± 0.04 m²/g to 176.75 ± 4.36 m²/g). The specific area of the pristine filter was 3.32 – 3.50 m²/cm³, while the specific area of composite filter was 360.30 – 378.51 m²/cm³. Both of the specific area and BET surface area of the composite filter are two order of magnitude higher than the pristine filter, and as a result, the contact between the aerosol particles and the composite filter were improved, which may improve the filtration efficiency.^{6,16}

Airborne particles filtration performances of the filters

In Fig. S3 (supporting information), the mean particle size of SiO₂ used for gas filtration was 296 nm, and it peaked at 240 nm, 30.01%. The most penetrating particle size (MPPS) is generally considered for particles under 300 nm, which gives the minimum efficiency of the filters.⁶ Thus, the air particles filtration performance of both the pristine filter and the composite filter were tested using SiO₂.

Fig. 5 shows the pressure drop, retention rate as a function of filtration time and Q_f , pressure drop as a function of gas flow rate of the pristine filter and the composite filter respectively. In Fig. 5a, with increasing filtration time (from 5 min to 120 min), the pristine filter showed retention rate of 68.04% at 5 min and above throughout the filtration experiment, and reached 79.88% at 120 min, while the composite filter showed the increasing retention rate from 99.9352% to 99.9999%. The SiO₂ particles were more likely to clog the pores of the pristine filter with the increasing filtration time (SiO₂ particles permeated the interior of the pristine filter, “deep filtration”, Fig. 6b), leading to a sharply increased pressure drop (from 1.68 kPa to 13.06 kPa) and far above the composite filter (from 0.97 kPa to 4.85 kPa). By contrast, the large amount of SiO₂ particles were captured on the surface and around the pores of the composite filter due to increased BET surface area (SiO₂ particles were trapped on the surface of the composite filter, “surface filtration”, Fig. 6c-e), which resulted in a much lower pressure drop of the composite filter. With increasing filtration time, more and more SiO₂ particles were accumulated on the surface of the filters and clogged their pores (Fig. 6), leading to SiO₂ cake layers gradually formed on the surface of all the filters.¹⁹ The small pore size between the particles of the cake on both the pristine filter and the composite filter could be conducive to obstructing smaller aerosol particles from passing through the filters, leading to

enhanced retention rate and high pressure drop.^{6, 33-34}

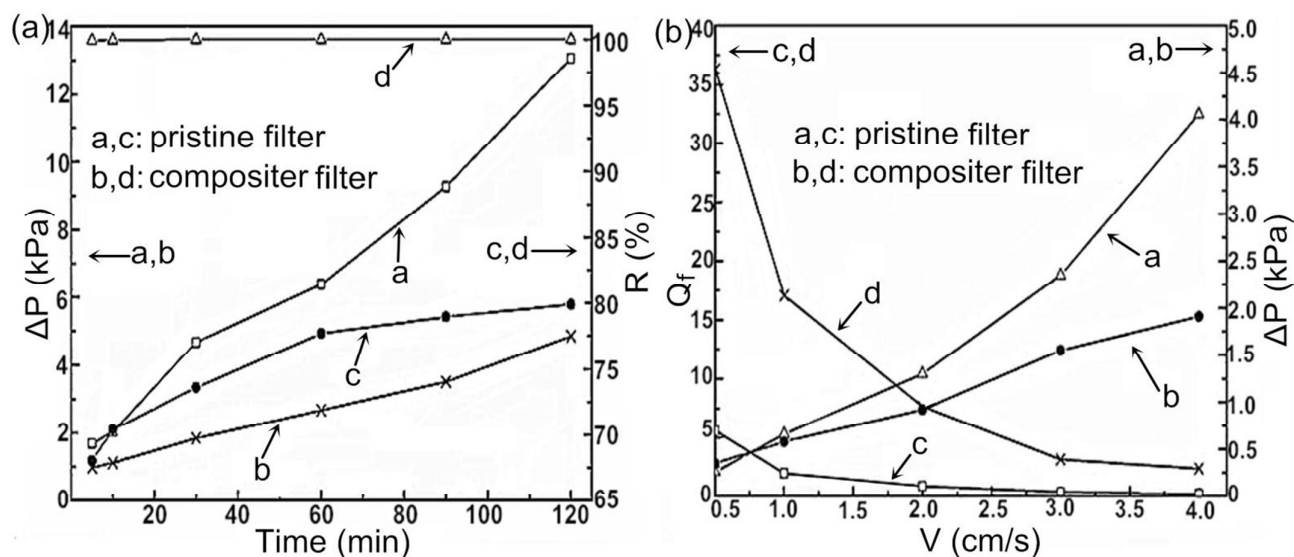
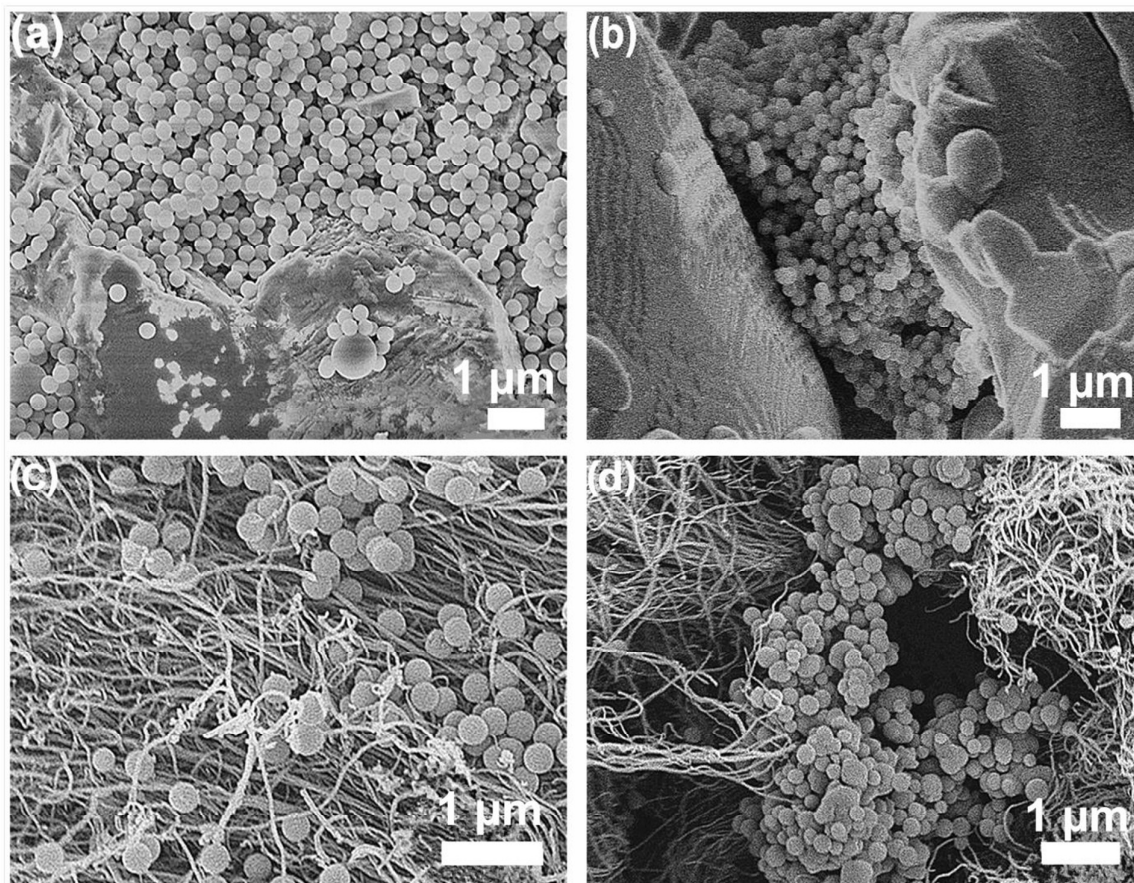


Fig. 5 (a) at the gas flow rate of 2 cm/s, a and b were the pressure drop varying with filtration time of the filters, while c and d were the retention rate varying with filtration time of the filters. **(b)** a and b were the pressure drop varying with gas flow rate of the filters, while c and d were the Q_f varying with gas flow rate of the filters.

From Fig. 5b, the pressure drop and Q_f of the pristine filter and the composite filter increased and decreased with the increasing gas flow rate, respectively, and the pressure drop of the pristine filter was always higher than the composite filter except at the very beginning through the whole filtration progress. It may be caused by the grown MWCNTs on the surface and around the pores of the composite filter, leading to smaller porosity and pore size.¹⁶ However, with the increasing gas flow rate, the pressure drop of the pristine filter increased sharply (from 0.26 kPa to 4.06 kPa) compared with the composite filter (from 0.35 kPa to 1.91 kPa) because a mass of SiO_2 particles with the high gas velocity could accumulated on the surface and clogged the pores of the pristine filter sharply³⁵⁻³⁸ (“deep filtration”, Fig. 6a-b). It led to a significantly decreased in porosity and the pore size of the pristine filter, while plenty of SiO_2 particles were deposited and captured by the MWCNTs on the surface and around the pores of the composite filter with their huge specific area and BET surface area (“surface filtration”, Fig. 6c-e), which made less pores of the composite filter with the clogging SiO_2 particles. Another reason why the composite filter has a much lower pressure drop is that the MWCNTs coated filter has a negligible effect on the pressure drop while the gas flow rate is low during air filtration,^{5, 39} and there is a gas velocity at the surface of the MWCNTs (owing

to the “slip effect”),⁴⁰⁻⁴¹ and the “slip effect” can reduce the drag force due to the MWCNTs on the gas flow.^{6, 40-41} The air flow around the MWCNTs is in the free molecular flow (FMF) regime, which can get a higher filtration efficiency with a lower pressure drop.^{6, 39} A higher value of quality factor (Q_f) implies a lower aerosol penetration and a better filtration performance of the filter.³³ Through the whole air filtration progress, with the increasing air flow rate, the value of Q_f for the composite filter (from 36.33 to 2.35) is always higher than the pristine filter (from 5.57 to 0.18, Fig. 5b), indicating that the MWCNTs play an important role in air filtration.⁵⁻⁶ With the air flow rate increasing, Brownian diffusion gets weak or can be neglected, and direct interception is the leading mechanism at a high gas flow rate. In other words, the SiO₂ particles have less time to deposit or be captured by the filters, which results in an unsatisfactory filtration performance.^{5, 42-43} Therefore, low gas filtration rate such as 0.5 cm/s can be conducive to achieving a high value of Q_f .



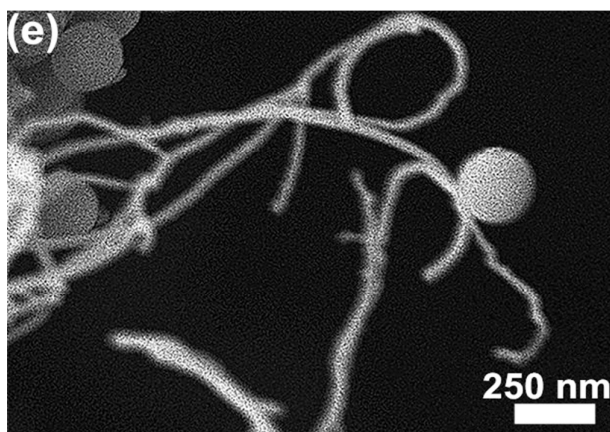


Fig. 6 FESEM images of the filters after gas filtration. (a) and (b) were SiO₂ particles accumulated on the surface and clogged the pore of the pristine filters respectively, while (c) and (d) were SiO₂ particles accumulated on the surface of the composite filter and the MWCNTs grown around the pore of the composite filter with the captured SiO₂ particles respectively. (e) High magnification view of the MWCNTs grown on the composite filter with the captured SiO₂ particles.

Fig. S4 (supporting information) shows the relationship between the gas velocity and retention rate of filters. From Fig. S4, the retention rate of both the pristine filter and the composite filter decreased with the increasing air flow rate, which also verifies the high rate of air flow against the filtration performance. The retention rate of the pristine filter decreased from 76.58% to 51.83%, while the composite filter only decreased from 99.9997% to 98.8724%. Apparently, the pristine filter is more sensitive to the air flow rate without the CNTs coating, and the retention rate of the composite filter is much higher than the criterion of HEPA filters (99.97% for 0.3 μm aerosol particles) by two orders of magnitude.⁷ The large BET surface area improved the retention rate of the composite filter, reducing the retention rate by 1.13% compared to 24.67% of pristine filter with the increasing air flow rate.

Retention rate and pressure drop as a function of the thickness of the pristine filter and the composite filter are shown in Fig. S5 (supporting information). For both the pristine filter and the composite filter, retention rate (for the pristine filter: from 67.61% to 85.89%, for the composite filter: from 99.9751% to 99.9999%) and pressure drop (for the pristine filter: from 1.30 kPa to 5.87 kPa, for the composite filter: from 0.98 kPa to 2.25 kPa) increased with the increasing thickness of the filters (the pristine filter: from 1 mm to 3 mm, the composite filter: from 1.17 mm to 3.22 mm). The increasing thickness of the pristine filter and the composite filter are conducive to retention rate

during air filtration, whereas the pressure drop of the pristine filter increased sharply and linearly compared with the MWCNTs coated filter, owing to the increasing thickness of the filters which change the shape and structure of the pores on the filters. At the gas flow rate of 2 cm/s and the thickness of 3.22 mm, the composite filter met the standard of ULPA with a very low pressure drop (2.25 kPa) compared with the pristine filter.

For different preparation time of the composite filter, the relationship between the gas velocity and the pressure drop is shown in Fig. S6 (supporting information). The amount of the MWCNTs grown on the composite filter increased with the extension of MWCNTs growth time, leading to the pressure drop of the filters (preparation time of the composite filter: 0 min (the pristine filter), 20 min, 40 min and 60 min) gradually decreased at each gas flow rate (from 1.0 cm/s to 4.0 cm/s), and the pressure drop increased with the increasing gas flow rate for all the filters (preparation time of the composite filter: 0 min (the pristine filter), 20 min, 40 min and 60 min). It verified that the MWCNTs grown on the composite filter and the low gas filtration rate played an important role in decreasing the pressure drop of the filters, and these results are consistent with the airborne particles filtration test (Fig. 5b, line a and b).

Antibacterial test of the pristine filter and the composite filter

Escherichia coli is one of the most common causative pathogens for human beings,⁴⁴⁻⁴⁵ and we used the typical bacteria (*E.coli*, ATCC 25922) to test the the antibacterial property of the filters.⁹ Both the pristine filter and the composite filter were used respectively to test their antibacterial properties. After shaking incubation at 37 °C for 40, 80 and 120 min, the pristine filter did not show any obvious change of bacteria colonies on the nutrient agar plate (about 2100 colonies per plate, Fig. 7a) for each test time (40, 80 and 120 min). In other words, the pristine filter did not have any remarkable antibacterial effects.

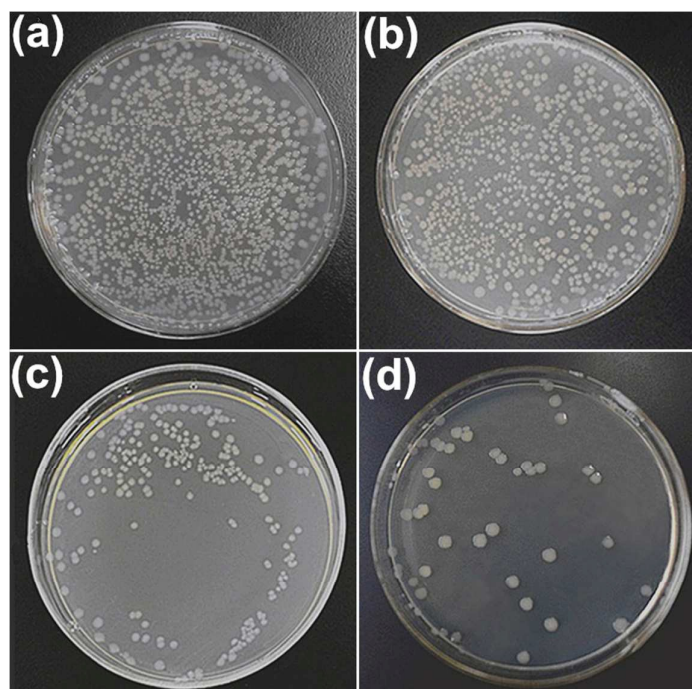


Fig. 7 Digital images of antibacterial effects. **(a)** The antibacterial results of the pristine filter for 40, 80 and 120 min. **(b)**, **(c)** and **(d)** were the antibacterial results of the composite filter for 40, 80 and 120 min respectively.

For the composite filter, the antibacterial property at each test time is shown in Fig. 7b-d and Fig. 8. Compared with the pristine filter, the antibacterial rate at each test time for the composite filter were 61.90% (40 min), 88.57% (80 min) and 97.86% (120 min). With increasing shaking incubation time, more *E. coli* are in contact with the CNTs, resulting in the inactivation of cells,²⁵ and thus higher antibacterial rate (Fig. 8). In Fig. 2d, the inner diameter of the MWCNTs prepared was only about 8.3 nm. The smaller the size and larger specific surface area of the CNTs, the higher the interaction between the living cells and the CNTs, resulting in a higher antibacterial rate caused by the damages of bacterial cell membranes.²⁵⁻²⁷ During air filtration, the number of bacteria in the air decreases by contacting with the composite filter,²⁵ and the size of bacteria is usually in micron order, which makes it hard to pass through the small filter pores and been inactivated by contacting with the MWCNTs grown on the composite filter.

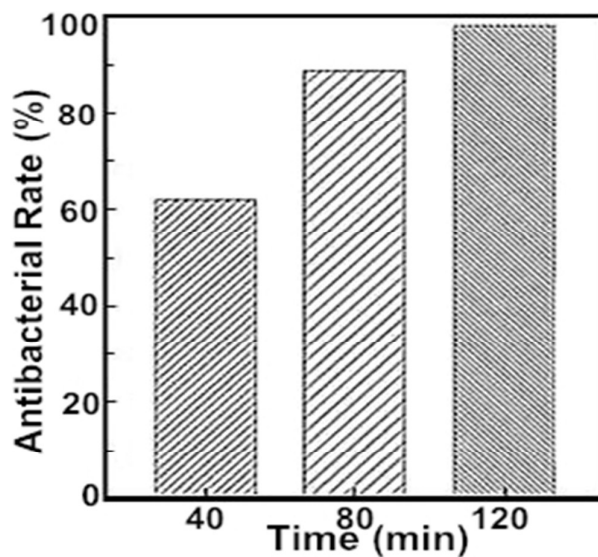


Fig. 8 Antibacterial rate of the composite filter at different test time (40, 80 and 120 min).

Water contact of angle on the pristine filter and the composite filter

To study the water repellency of the pristine filter and the composite filter, we tested the water contact angle on the pristine filter and the composite filter (Fig. 9). The water contact angle on the pristine filter was only 3.6° , and the water was absorbed immediately when dropped due to the hydrophilic and porous surfaces of the pristine filter (Fig. 9a). In contrast, the high water contact angle (148.2° , Fig. 9b) in the composite filter indicates high water repellency (hydrophobic), which keeps the surfaces of the composite filter dry and improves the antibacterial capability of the composite filter since dry conditions are less suitable for bacteria growth. It is also tough for bacteria to develop biofilms without enough water.⁴⁶⁻⁴⁸ Benefited from the high antibacterial property and high water repellency of MWCNTs, the lifespan of the composite filter is greatly extended without damage by the bacterial activities on the composite filter. Besides that, with the dry condition and antibacterial property, the micro-organisms is not easy to breed and adhere to accumulate dust on the composite filter, which creates few bad odours and improves the quality of air filtration.²⁸ The hydrophobic surface of the composite filter leads to few dust cohering with each other, implying that it is easier to clean after air filtration. Furthermore, with the high surface hydrophobicity, the composite filter can also meet the needs of purified air for the people who live in moist areas such as coastal areas or regions with tropical rain forest climate.¹⁶



Fig. 9 Images of surface hydrophobic behaviour of the pristine filter and the composite filter. **(a)** The water contact angle on the pristine filter. **(b)** The water contact angle on the composite filter.

Conclusions

In this paper, we have fabricated the composite filter by growing MWCNTs on the alumina ceramic membranes via CVD method. The air filtration efficiency of this filter was significantly improved, meeting both criteria of HEPA and ULPA under the air filtration conditions investigated. The composite air filter has a much lower pressure drop indicating lower energy requirement. Moreover, the high water repellency and antibacterial rate improve the ease of removal of the cake layers of the composite filter after air filtration, and this composite filter can be widely used no matter in domestic places, commercial places or industrial places.

Acknowledgements

Financial support was provided by the National Natural Science Foundation of China (21276124), Jiangsu Province scientific supporting project (BE2014717).

Notes and References

1. Bert Brunekreef, *Procedia Social and Behavioral Sciences*, 2010, 41, 6661-6669.
2. Gilda Rusu-Zagar, Catalin Rusu-Zagar, Ionel Iorga, Andrei Iorga, *Procedia Social and Behavioral Sciences*, 2013, 92, 826-831.
3. Jonathan O. Anderson, Josef G. Thundiyil, Andrew Stolbach, *J. Med. Toxicol.*, 2012, 8, 166-175.
4. Mitsakou C, Housiadas C, Eleftheriadis K, Vratolis S, Helmis C, Asimakopoulos D, *Indoor Air*, 2007, 17(2), 143-152.

5. Hamed Parham, Steven Bates, Yongde Xia, Yanqiu Zhu, *Carbon*, 2013, 54, 215-223.
6. Peng Li, Chunya Wang, YingYing Zhang, Fei Wei, *Small*, 2014, 10(22), 4543-4561.
7. A. Bennett, *Filtr.Separat.*, 2012, 49, 22.
8. H. G. Horn, Proceedings of the Seventh World Filtration Congress, Budapest, 1996.
9. Jae Hee Jung, Gi Byoung Hwang, Jung Eun Lee, Gwi Nam Bae, *Langmuir*, 2011, 27, 10256-10264.
10. Jian Hu, Zhaoxiang Zhong, Feng Zhang, Weihong Xing, Ze-Xian Low, Yiqun Fan, *Ceramics International*, 2015, 41(5), 7080-7090.
11. Gi Byoung Hwang, Kyoung Mi Sim, Gwi-Nam Bae, Jae Hee Jung, *Journal of Aerosol Science*, 2015, 86, 44-54.
12. Hongxu Gao, Feng Houa, Xuerong Zhenga, Jiachen Liua, Anran Guoa, Deming Yanga, Yuxuan Gongb, *Vacuum*, 2015, 112, 1-4.
13. Venkata K.K. Upadhyayula, Shuguang Deng, Martha C. Mitchell, Geoffrey B. Smith, *Science of the Total Environment*, 2009, 408(1), 1-13.
14. Kaufui V. Wong, Benoit Bachelier, *Journal of Energy Resources Technology*, 2013, 136(2), 021601.
15. Xitong Liu, Mengshu Wang, Shujuan Zhang, Bingcai Pan, *Journal of Environmental Sciences*, 2013, 25(7), 1263-1280.
16. Peng Li, Yichen Zong, Yingying Zhang, Mengmeng Yang, Rufan Zhang, Shuiqing Li, Fei Wei, *Nanoscale*, 2013, 5, 3367.
17. Dóra Fejes, Klára Hernádi, *Materials*, 2010, 3, 2618-2642.
18. Liu G.Y., Zhong D.Y., Xia S.H., Cheng S.F., Ding Y.G., Lu Y.J., Shao Y.J., Li H.Y., Hangfu, L.J., Wang E.G., *Applied Surface Science*, 2003, 215, 209-213.
19. Zhaoxiang Zhong, Weihong Xing, Xin Li and Feng Zhang, *Ind. Eng. Chem. Res.*, 2013, 52(15), 5455-5461.
20. M.Lee, Z.Wu, K.Li, *Advances in Membrane Technologies for Water Treatment*, 2015, a volume in Woodhead Publishing Series in Energy, 43-82.
21. HyukHee Hana, Seung Hee Ryua, Shin-ichi Nakaob, Yong Taek Lee, *J. Membr Sci.*, 2013, 431, 72-78.
22. Liu C, Hsu PC, Lee HW, Ye M, Zheng G, Liu N, Li W, Cui Y, *Nat Commun.*, 2015, 6, 6205.

23. Zahra Soleimani, Najmeh Parhizgari, Hassan Dehdari Rad, Mohammad Reza Akhoond, Majid Kermani, Mohammad Bagherian Marzouni, Hamed Goudarzi, Gholamreza Goudarzi, *Aerobiologia*, 2015, 31, 127-141.
24. Aaron J. Prussin, Ellen B. Garcia, Linsey C. Marr, *Environmental Science & Technology Letters*, 2015, 2, 84-88.
25. Seoktae Kang, Moshe Herzberg, Debora F. Rodrigues, and Menachem Elimelech, *Langmuir*, 2008, 24, 6409-6413.
26. Nel. A, Xia.T, Madler. L, Li.N, *Science*, 2006, 311, 622-627.
27. Guang Jia, Haifang Wang, Lei Yan, Xiang Wang, Rongjuan Pei, Tao Yan, Yuliang Zhao, and Xinbiao Guo, *Environ. Sci. Technol.*, 2005, 39, 1378-1383.
28. R. S. Barhate , Seeram Ramakrishna, *J. Membr Sci.*, 2007, 296(1-2), 1-8.
29. J.C. Ruiz, Ph. Blanc, E. Prouzet, P. Coryn, P. Laffont, A. Larbot, *Separation and Purification Technology*, 2000, 19, 221-227.
30. T. Belin, F. Epron, *Materials Science and Engineering B*, 2005, 119, 105-118.
31. Liliane Bokobza, Jean-Luc Bruneel, Michel Couzi, *Vibrational Spectroscopy*, 2014,74, 57-63.
32. H. Hiura, T. Ebbesen, K. Tanigaki, H. Takahashi, *Chemical Physics Letters*, 1993, 202, 509.
33. C. Y. Chen, *Chem. Rev.*, 1995, 55, 595-623.
34. C. YANG, Chinese. *J. Chem.Eng.*, 2012, 20(1), 1-9.
35. D. C. Walsh, J. I. T. Stenhouse, K. L. Scurrah and A. Graef, *J. Aerosol Sci.*, 1996, 27(suppl.1), S617-S618.
36. A. Bredin, B. J. Mullins, *Separation and Purification Technology*, 2012, 90, 53-63.
37. C. B. Song, H. S. Park and K. W. Lee, *Powder Technol.*, 2006, 163,152-159.
38. S. Payet, D. Boulaud, G. Madelaine and A. Renoux, *J. Aerosol Sci.*, 1992, 23,723-735.
39. B. Maze, H. Vahedi Tafreshi, Q. Wang, B. Pourdeyhimi, *J. Aerosol. Sci.*, 2007, 38, 550.
40. D. Shou, L. Ye, J. Fan, *Polymer*, 2014, 55, 3149.
41. C.-H. Hung, W.W.-F. Leung, *Sep. Purif. Technol.*, 2011, 79, 34.
42. Guan. Tianjia, Yao.Maosheng, *J. Aerosol Sci.*, 2010, 41(6), 611-20.
43. André Larbot, Marielle Bertrand, Sonia Marre, Eric Prouzet, *Separation and Purification Technology*, 2003, 32, 81-85.
44. Mehdi Alboofetile, Masoud Rezaei, Hedayat Hossein, Mehdi Abdollah, Philadelphia, *Food*

Control, 2014, 36, 1-7.

45. J. O. Noyce, H. T. Michels and C. W. Keevil, *J. Hosp. Infect.*, 2006, 63, 289-297.
46. C. Espirito Santo, N. Taudte, D. H. Nies and G. Grass, *Appl. Environ. Microbiol.*, 2008, 74, 977-986.
47. P.-T. Chiang, G.-J. Chen, S-R. Jian and Y-H. Shih, *Materials Technology*, 2012, 27(1), 107-109.
48. Divya N. Amin, Gerald L. Hazelbauer, *Journal of biological Chemistry*, 2012, 287, 41697-41705.
49. Bendi Ramaraju, Toyoko Imae, Addisu Getachew Destaye, *Applied Catalysis A: General*, 2015, 492, 184-189.
50. Lifeng Zhang, Jie Luo, Todd J. Menkhaus, Hemanthram Varadaraju, Yuyu Sun, Hao Fong, *Journal of Membrane Science*, 2011, 369, 499–505.